

# Millimeter Wave Doppler Sensor for Nondestructive Evaluation of Materials

S. Liao, S. Bakhtiari, T. Elmer, B. Lawrence, E. R. Koehl, N. Gopalsami, and A. Raptis

Argonne National Laboratory  
9700 S. Cass Avenue, Lemont, IL, 60439  
(630) 252-8982; fax (630) 252-3250; e-mail [bakhtiari@anl.gov](mailto:bakhtiari@anl.gov)

## INTRODUCTION

Resonance modes are intrinsic characteristics of objects when excited at those frequencies. Probing the resonance signatures can reveal useful information about material composition, geometry, presence of defects, and other characteristics of the object under test. Vibration spectra can be measured remotely with high degree of sensitivity using a millimeter wave (mmW) Doppler sensor and a remote excitation source. This novel nondestructive evaluation (NDE) method can work in a non-contact manner as an alternative or complementary approach to conventional NDE methods such as those based on acoustic/ultrasonic and optical techniques. Millimeter wave vibrometry can be used for a wide range of civil and national security applications. Examples include detection of defects and degradation for diagnostics and prognostics of materials components and rapid standoff inspection of shielded/sealed containers for contraband. In this paper, we evaluate the performance of a compact mmW vibrometer developed at Argonne. Our 94 GHz I-Q Doppler sensor monitors the mechanical vibration signature of the object under interrogation that is induced by continuous wave excitation. For proof-of-principle demonstrations, the test objects were mechanically excited by an electronically controlled shaker using sinusoidal waves at various frequencies ranging from DC to 200 Hz. We will present a number of laboratory test results and will discuss the method's applicability to some practical NDE applications.

## Resonance Signatures

Vibration eigen-modes at certain natural resonant frequencies are unique characteristics of an object experiencing mechanical excitation [1]. These eigen-modes and natural resonant frequencies are determined by the equivalent inertia mass  $M_{eff}^m$  and stiffness  $k_{eff}^m$ , obeying the following law of physics,

$$M_{eff}^m(z) \frac{d^2 \Delta}{dz^2} + k_{eff}^m(z) \Delta = 0 \quad (1)$$

where  $z$  is the axial coordinate of the object, e.g., axis of a cylinder and  $\Delta$  is the vibration amplitude of the eigen-modes. Different eigen-modes have different values of  $M_{eff}^m$  and  $k_{eff}^m$  for the  $m^{\text{th}}$  azimuthal eigen-mode number, thus giving rise to different eigen-mode patterns and natural resonant frequencies. In order to solve Eq. (1), boundary conditions have to be specified, e.g., free standing, simply support or clamped. As an example, using the boundary conditions associated with a free standing, empty cylinder, the natural resonant frequencies can be obtained from Eq. (1) resembling a simple oscillator,

$$\omega_{m,n} = n \sqrt{\frac{k_{eff}^m}{M_{eff}^m}} \quad (2)$$

where  $n$  is the axial eigen-mode number. From Eq. (2), the resonance frequency depends on the effective mass  $M_{eff}^m$  and the effective spring constant  $k_{eff}^m$ , both of which strongly depend on the geometry, material and boundary conditions of the object under evaluation. Through measurement of the resonance signatures, frequency shift and number of resonances can effectively reveal information about the attributes of the object.

## Millimeter Wave Doppler Sensor

Our prototype millimeter Wave (mmW) sensor works at 94 GHz [2], providing a unique combination of

sensitivity and long range for detection of vibration signals [3]. Compared to microwave techniques [4]-[28], mmW range has the advantages of a) shorter wavelengths providing greater sensitivity to small displacements and b) higher spatial resolution obtainable with a reasonable aperture size. Compared to laser Doppler technique, the main advantages of the mmW frequency range for remote sensing [3] include a) penetration through many optically opaque dielectric materials, b) low atmospheric attenuation allowing long-range operation, c) low sensitivity to surface condition of the object (optically coarse reflecting surfaces), and d) ease of alignment.

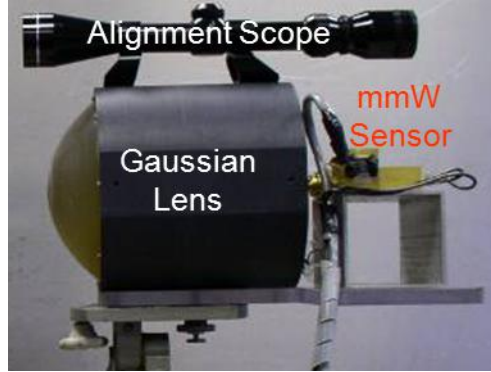


**Fig. 1: 94-GHz Doppler vibrometer with a Gaussian focus lens and an alignment scope.**

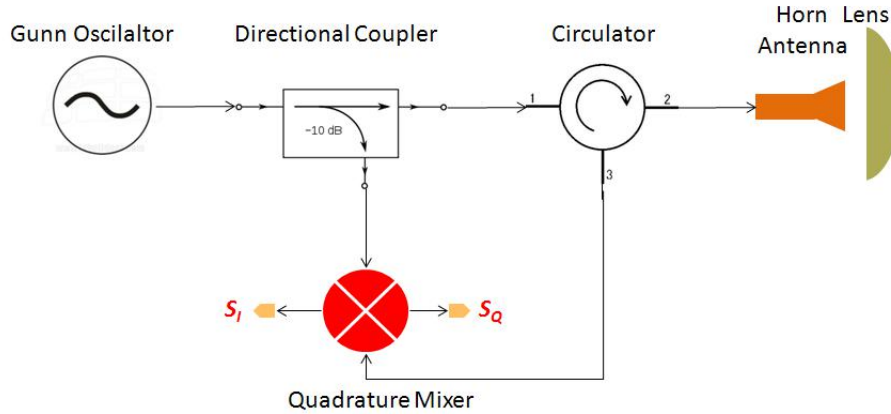


**Fig. 2: Functional block diagram of the 94-GHz Doppler vibrometer with a Gaussian optic lens antenna.**

A picture of the 94-GHz Doppler sensor system is shown in Fig. 1 and its functional block diagram is shown in Fig. 2. A W-band solid-state Gunn oscillator generates the reference and transmitted mmW signal. A fraction of the signal is fed to one of the inputs of the I-Q quadrature mixer. The remainder of the signal is fed to a circulator and corrugated horn antenna (2.39 mm in diameter) and is focused by a 6-inch-diameter dielectric lens on the target. The antenna system has a gain  $>25.0$  dBi and a beam angle  $\sim 1$  degree. The reflected mmW signal is fed to the other input of the of the I-Q mixer, and is down-converted (homodyne) to both direct and quadrature channels, i.e.,  $(S_I, S_Q)$ . The phase  $\varphi(t)$  can be expressed as [2]-[3],

$$S_I = A(t) \cos[\varphi(t)] \quad (3)$$

$$S_Q = A(t) \sin[\varphi(t)] \quad (4)$$

where  $A(t)$  is the amplitude and  $\varphi(t)$  is the associated phase. Combining Eq. (3) and Eq. (4) gives

$$\varphi(t) = \arctan \left[ \frac{S_Q}{S_I} \right] \quad (5)$$

The signal or  $\varphi(t)$  contains the object's Doppler frequency  $f_d(t)$  information,

$$f_d(t) = \frac{1}{2\pi} \frac{d\varphi(t)}{dt} \quad (6)$$

### EXPERIMENTAL SETUP

The experimental setup for the mmW Doppler vibrometer is shown in Fig. 3. A picture of the laboratory components is shown in Fig. 4. A shaker is frequency-swept by a function generator from DC to 500 Hz, during a time period of  $T = 999$  seconds. The frequency response of the object under evaluation is continuously monitored by the mmW system in real time. Both the voltage signal from the function generator and the I/Q signals ( $S_I, S_Q$ ) from the mmW sensor are collected by LabVIEW™ software running on a Personal Computer (PC).

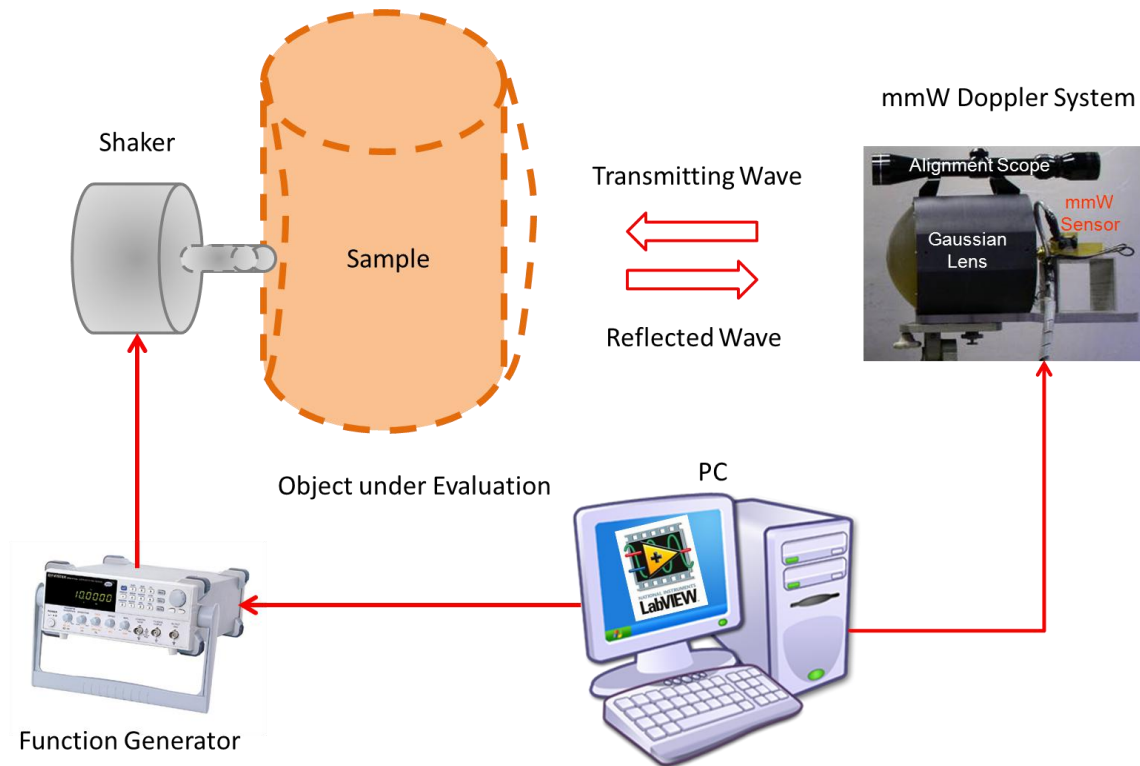


**Figure 3: Experimental setup for resonance signature measurement using a mmW Doppler sensor.**

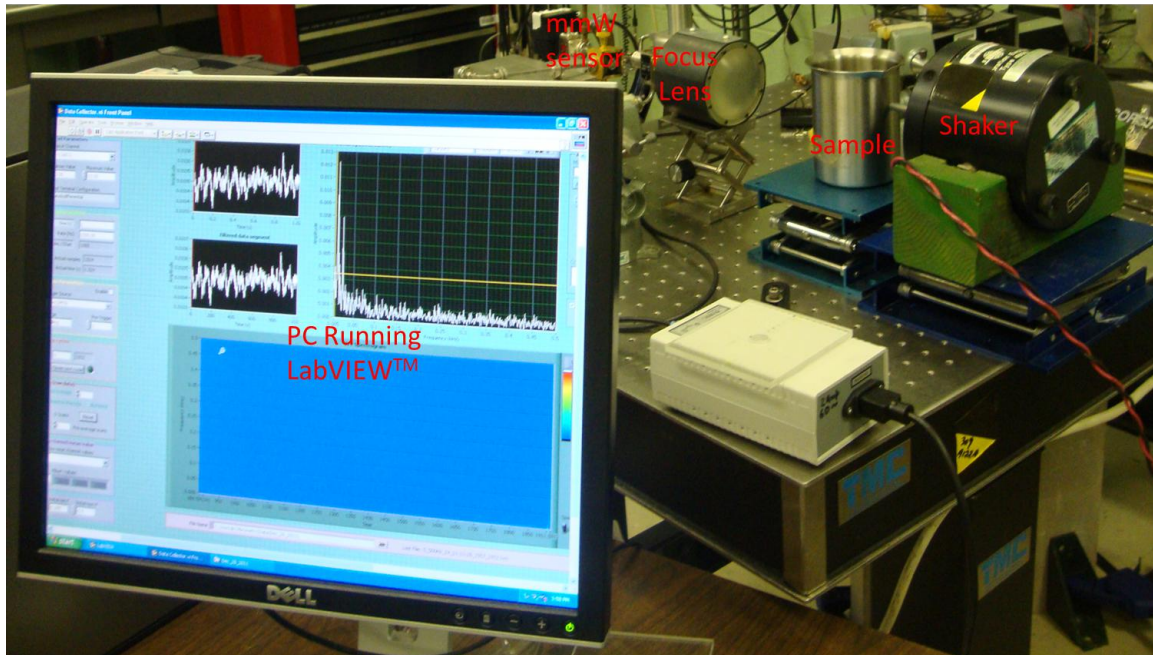


Figure 4: Laboratory photo of the experimental setup shown in Fig. 3.

## EXPERIMENTAL ASSESSMENTS

Two typical sets of experiments were carried out to assess the performance of the resonance signature NDE method; 1) simulated defects in plates made of different materials (plastic and aluminum), and 2) a cylindrical steel can loaded with different materials (water, and oil).

### Simulated Defects

Two types of manufactured defects have been investigated: circular and rectangular defects of different sizes on a) a 4-inch-by-4-inch aluminum plate, and b) a 4-inch-by-4-inch plastic plate. In all experiment, the plates were clamped on both sides as constraint support. Fig. 5 shows the resonance signatures for circular defects of case a): the resonant frequencies, as marked on each frequency spectra, are clearly different for the plate without (green) and with a  $\frac{1}{4}$ -inch diameter circular defect (blue), and with a  $\frac{1}{2}$ -inch diameter circular defect (red). An example resonance frequency triplet from Fig. 5 is (61.52 Hz, 64.45 Hz, 66.41 Hz). Fig. 6 shows results for the rectangular defects for: the plate without defect (green), with  $\frac{1}{8}$ -inch by  $\frac{1}{2}$ -inch defect (blue), and with  $\frac{1}{4}$ -inch by  $\frac{1}{2}$ -inch defect (red). An example resonance frequency triplet from Fig. 6 is (49.80 Hz, 42.97 Hz, 41.99 Hz). Similarly, Fig. 7 and Fig. 8 show the results for case b). Once again the resonant frequency shifts are clearly observable. Example resonance frequency triplets for Fig. 7 and Fig. 8 are (89.84 Hz, 88.87 Hz, 83.01 Hz) and (41.99 Hz, 38.09 Hz, 40.04 Hz) respectively.

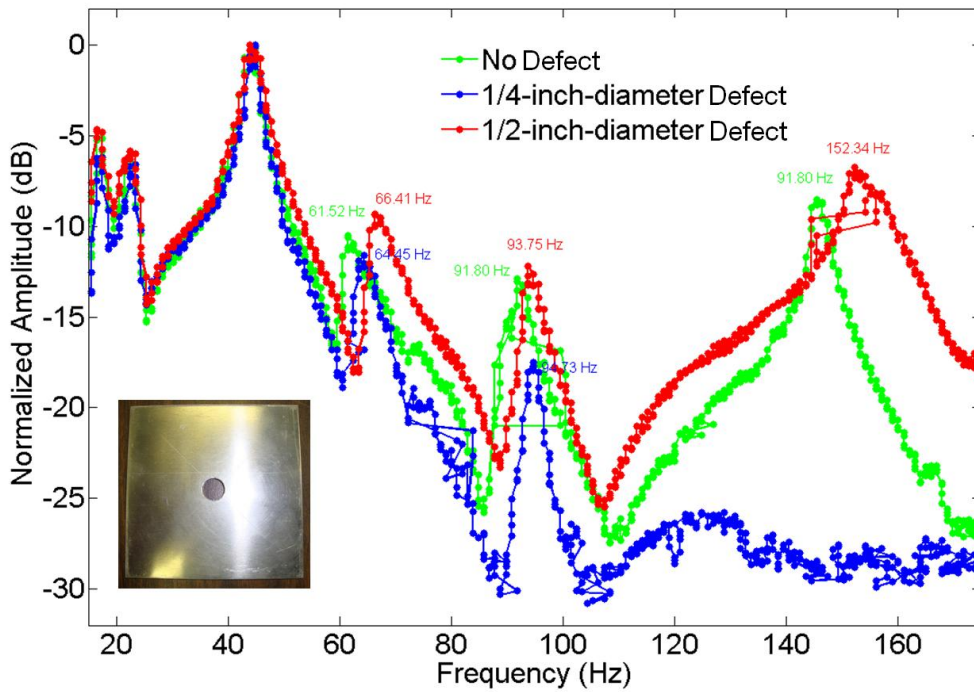


Figure 5: Resonance signatures of a 4-inch-by-4-inch aluminum plate with manufactured circular defects. Also shown is the photo of a representative sample, i.e., a 1/2-inch circular defect.

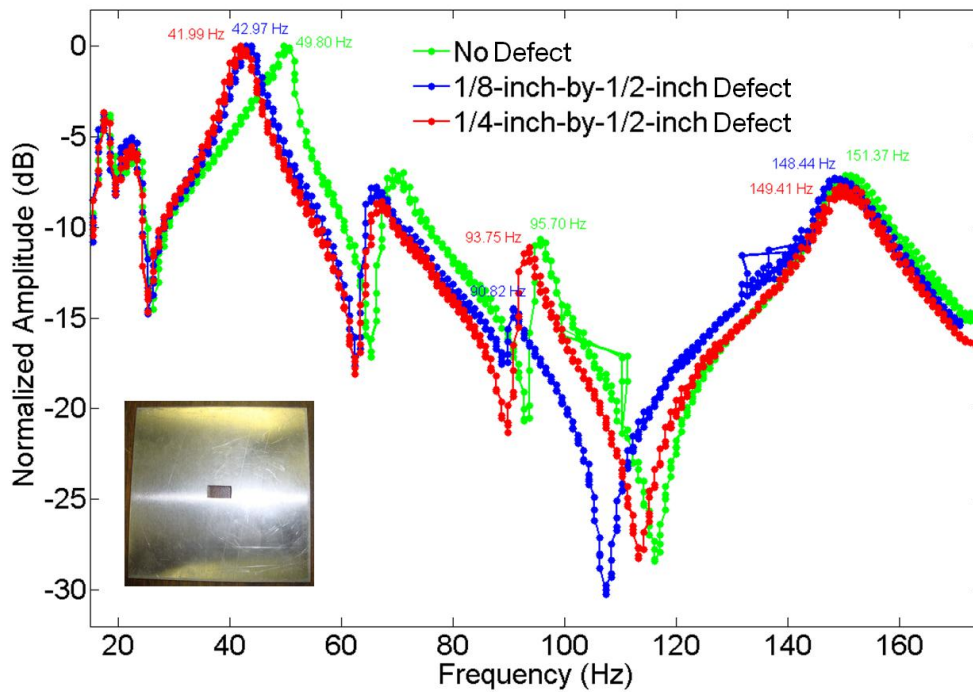


Figure 6: Resonance signatures of a 4-inch-by-4-inch aluminum plate with manufactured rectangular defects. Also shown is the photo of a representative sample, i.e., a 1/4-inch-by-1/2-inch rectangular defect.

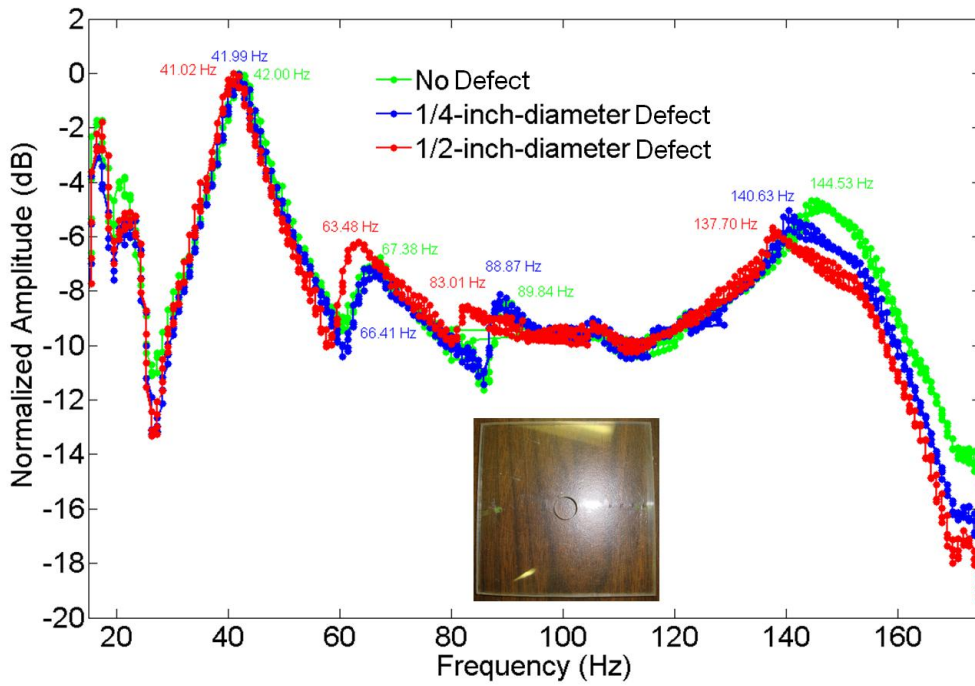


Figure 7: Resonance signatures of a 4-inch-by-4-inch plastic plate with manufactured circular defects. Also shown is the photo of a representative sample, i.e., a 1/2-inch circular defect.

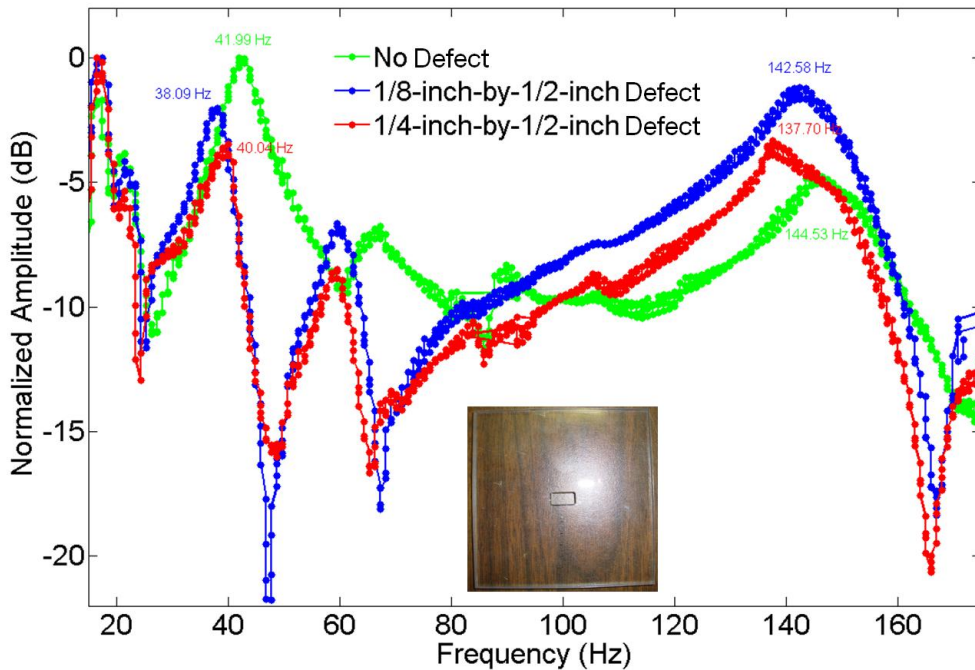


Figure 8: Resonance signatures of a 4-inch-by-4-inch plastic plate with manufactured rectangular defects. Also shown is the photo of a representative sample, i.e., a 1/4-inch-by-1/2-inch rectangular defect.

Loaded Container

A 3-inch-diameter, 4.5-inch long cylindrical steel can was used in the experiment for two cases: a) fully-filled and half-filled with water; and b) fully-filled and half-filled with mineral oil. Fig. 9 shows the experimental results for case a), from which the resonant frequency shift is clearly detectable. For the case when the steel can is fully-filled with water, the resonant frequency is 65.43 Hz, compared to 72.27 Hz when it is half-filled with water. Fig. 10 shows similar results for case b). For the case when the steel can is fully-filled with oil, the resonant frequency is 57.62 Hz, compared to 73.24 Hz when half-filled with oil.

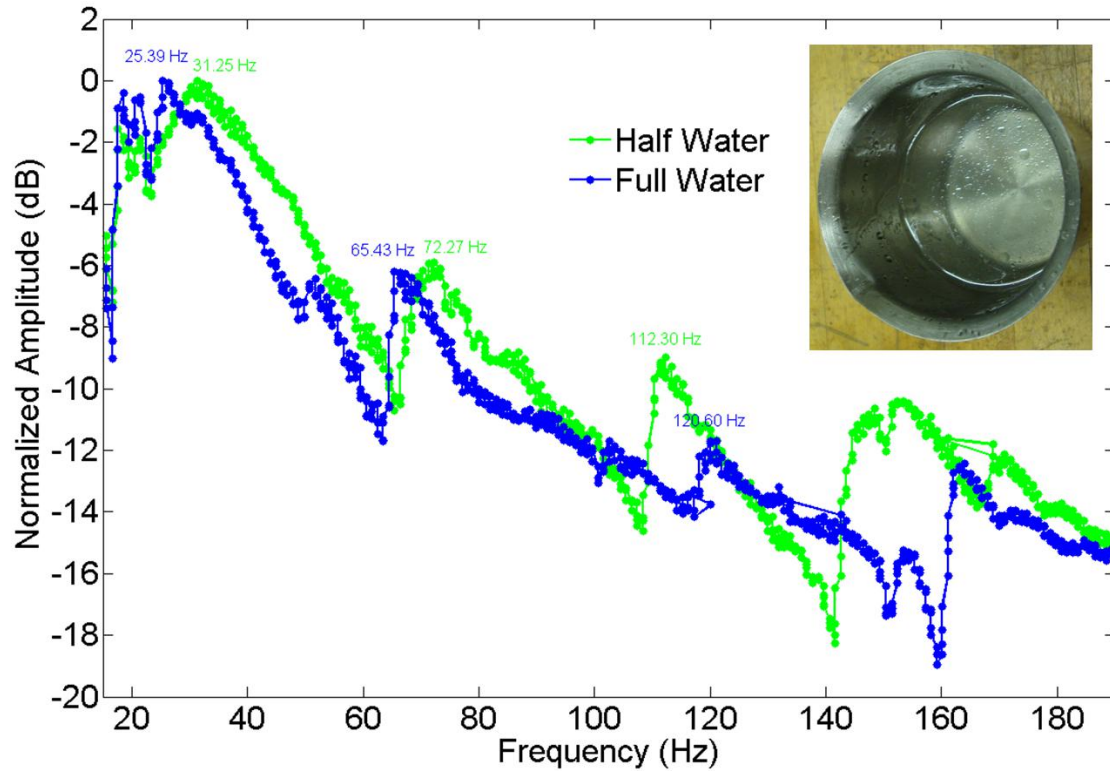
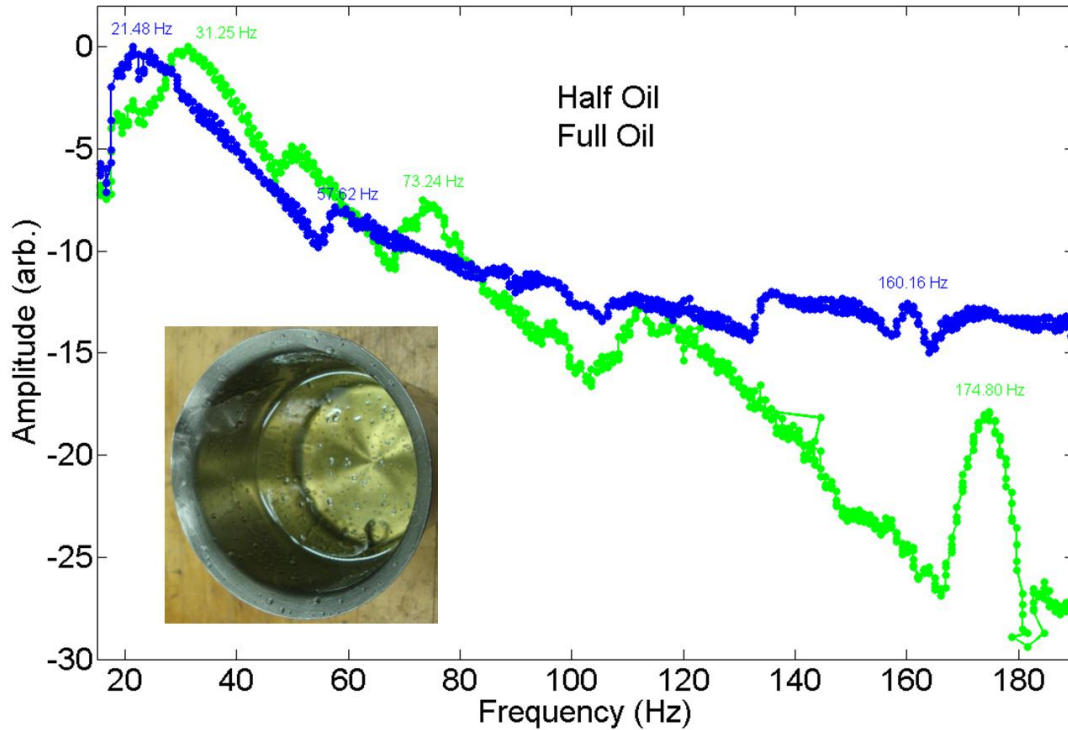


Figure 9: Resonance signatures for a water-filled cylindrical steel can with a diameter of 3 inches and a height of 4.5 inches.



**Figure 10: Resonance signatures for an oil-filled cylindrical steel can with a diameter of 3 inches and a height of 4.5 inches.**

## CONCLUSION

A novel NDE method has been investigated for noncontact characterization of materials and components. The results suggest that the method provides a practical and simple approach for a wide range of standoff sensing applications. The measured signals are unique characteristic resonances of the object under evaluation. A 94-GHz Doppler sensor was used to monitor the resonance signatures in real time. Two sets of experiments have been performed to show the performance of the method for NDE applications. The experiments consisted of 1) Simulated defects of different sizes and shapes on plates made of different materials such as plastic and aluminum and 2) shielded/sealed materials (water and oil) inside a cylindrical steel can. The experimental results clearly show unique resonance signatures for all the objects tested in this work. The resonance frequency shifts of up to a few Hz were easily detectable by the sensor system. Based on the results of the investigations to date, it can be concluded that this NDE method can be used in many civil and national security applications such as detecting defects in multilayer structures and identification of the contents of shielded/sealed materials inside containers. Ongoing investigations in this work are associated with incorporation of an air-coupled excitation source such as high-power speaker or a laser, which will readily enable the method to be implemented as a standoff NDE tool.

## REFERENCES

1. Lakis, A. A. and Paidoussis M. P., "Free Vibration of Cylindrical Shells Partially Filled with Liquid", *Journal of Sound and Vibration*, 19 (1) 1-15, 1971.
2. S. Bakhtiari, Shaolin Liao, T. Elmer, N. Gopalsami and A. C. Raptis, "A Real-time Heart Rate Analysis for a Remote Millimeter Wave I-Q Sensor", *IEEE Transactions on Biomedical Engineering*, vol. 58, pp. 1839-1845, 2011.
3. S. Bakhtiari, N. Gopalsami, T. W. Elmer and A. C. Raptis, "Millimeter wave sensor for far-field standoff vibrometry," *Review of Quantitative Nondestructive Evaluation*, American Institute of Physics, Vol. 28, 2009.
4. H. J. Kim, K. H. Kim, Y. S. Hong, and J. J. Choi, "Measurement of human heartbeat and respiration signals using phase detection radar," *Review of Scientific Instruments*, 78, 104703 (2007).



5. J. Lin and C. Li, "Wireless non-contact detection of heartbeat and respiration using low-power microwave radar sensor," *Proceedings of Asia-Pacific Microwave Conference*, 2007.
6. C. Li and J. Lin, "Random body movement cancellation in Doppler radar vital sign detection," *IEEE Transactions on Microwave Theory and Techniques*, Vol. 56, No. 12, December 2008.
7. D. T. Petkie, C. Benton and E. Bryan, "Millimeter wave radar for remote measurement of vital signs," *Radar Conference*, 2009 IEEE, 4-8 May (2009).
8. S. Liao, N. Gopalsami, S. Bakhtiari, T. W. Elmer, E. R. Koehl, and A. C. Raptis, "A novel interferometric sub-THz Doppler radar with a continuously oscillating reference arm," *IEEE Transactions on Terahertz Science and Technology*, vol. 4, no. 3, pp. 307 - 313, Mar. 2014. DOI: 10.1109/TTHZ.2014.2307165
9. S. Liao, Z. Wang, L. Ou, and Y. Peng, "A Harmonics Interferometric Doppler Sensor With a Neon Lamp Detector," *IEEE Sensors Journal*, pp. 1 - 1, 2020, DOI: 10.1109/JSEN.2020.2970055.
10. S. Bakhtiari, T. Elmer, M. Cox, N. Gopalsami, A. Raptis, S. Liao, I. Mikhelson and A. Sahakian, "Compact Millimeter-Wave Sensor for Remote Monitoring of Vital Signs," *IEEE Transactions on Instrumentation and Measurement*, vol. 61, no. 3, pp. 830 - 841, Mar. 2012, DOI: 10.1109/TIM.2011.2171589.
11. S. Bakhtiari, S. Liao, T. Elmer, N. Gopalsami, and A. C. Raptis, "A real-time heart rate analysis for a remote millimeter wave I-Q sensor," *IEEE Transactions on Biomedical Engineering*, vol. 58, no. 6, pp. 1839 - 45, Mar. 2011. DOI: 10.1109/TBME.2011.2122335
12. I. V. Mikhelson, S. Bakhtiari, T. W. E. II, S. Liao, and A. V. Sahakian, "Remote sensing of heart rate using millimeter-wave interferometry and probabilistic interpolation," in *Proceedings SPIE 8719, Smart Biomedical and Physiological Sensor Technology X*, 2013, vol. 87190M. DOI: 10.1117/12.2015282
13. S. Liao, N. Gopalsami, S. Bakhtiari, T. Elmer, and A. C. Raptis, "A novel interferometric millimeter wave Doppler radar," *2013 IEEE International Instrumentation and Measurement Technology Conference (I2MTC)*, Minneapolis, MN, 2013, pp. 387-391. DOI: 10.1109/I2MTC.2013.6555445
14. S. Liao et al., "Standoff through the wall sensing at Ka band," *Materials Evaluation, American Society of Nondestructive Testing*, vol. 70, no. 10, pp. 1136 - 1145, Oct. 2012.
15. S. Liao, S. Bakhtiari, T. Elmer, A. C. Raptis, I. V. Mikhelson, and A. V. Sahakian, "Millimeter-wave I-Q standoff biosensor," in *Proceedings SPIE 8371, Sensing Technologies for Global Health, Military Medicine, Disaster Response, and Environmental Monitoring II; and Biometric Technology for Human Identification IX*, 2012, vol. 83711D. DOI: 10.1117/12.924241
16. S. Liao and R. J. Vernon, "A fast algorithm for computation of electromagnetic wave propagation in half space," *IEEE Trans. on Antennas and Propagation*, vol. 57, no. 7, pp. 2068 - 2075, Jul. 2009. DOI: 10.1109/TAP.2009.2021890
17. S. Liao, "Miter bend mirror design for corrugated waveguides," *Letters of Progress in Electromagnetics Research*, vol. 10, pp. 157 - 162, 2009. DOI: 10.2528/PIERL09062103
18. S. Liao and R. J. Vernon, "Sub-THz beam-shaping mirror designs for quasi-optical mode converter in high power gyrotrons," *Journal of Electromagnetic Waves and Applications*, vol. 21, no. 4, pp. 425 - 439, 2007. DOI: 10.1163/156939307779367332
19. S. Liao and R. J. Vernon, "A fast algorithm for wave propagation from a plane or a cylindrical surface," *International Journal of Infrared and Millimeter Wave*, vol. 28, no. 6, pp. 479 - 490, 2007. DOI: 10.1007/s10762-007-9213-0
20. Liao S, Vernon RJ, Neilson J, "A four-frequency mode converter with small output angle variation for a step-tunable gyrotron," *Proceedings of the 15th Joint Workshop On Electron Cyclotron Emission and Electron Cyclotron Resonance Heating, Ec-15*. 477-482. DOI: 10.1142/9789812814647\_0068
21. N. Gopalsami, S. Liao, T. Elmer, E. Koehl, A. Heifetz, A. Raptis, L. Spinoulas, and A. Katsaggelos, "Passive millimeter-wave imaging with compressive sensing," *Optical Engineering*, vol. 51, no. 9, pp. 091614 - 1:9, Sep. 2012. DOI: 10.1117/1.OE.51.9.091614
22. S. Liao et al., "Passive millimeter-wave dual-polarization imagers," *IEEE Transactions on Instrumentation and Measurement*, vol. 61, no. 7, pp. 2042 - 2050, Feb. 2012. DOI: 10.1109/TIM.2012.2183032

23. S. Liao et al., "Nuclear radiation induced atmospheric air breakdown in a spark gap," *IEEE Transactions on Plasma Science*, vol. 40, no. 4, pp. 990 - 994, Mar. 2012. DOI: 10.1109/TPS.2012.2187343
24. S. Liao et al., "Microwave Remote Sensing of Ionized Air," *IEEE Geoscience and Remote Sensing Letters*, vol. 8, no. 4, pp. 617 - 620, Jul. 2011, DOI: 10.1109/LGRS.2010.2098016.
25. A. Heifetz, H. T. Chien, S. Liao, N. Gopalsami, and A. C. Raptis, "Millimeter-wave scattering from neutral and charged water droplets," *Journal of Quantitative Spectroscopy and Radiative Transfer*, vol. 111, no. 17 - 18, pp. 2550 - 2557, 2010. DOI: 10.1016/j.jqsrt.2010.08.001
26. S. Liao and R. J. Vernon, "A fast algorithm for computation of electromagnetic wave propagation in half space," *IEEE Trans. on Antennas and Propagation*, vol. 57, no. 7, pp. 2068 - 2075, Jul. 2009. DOI: 10.1109/TAP.2009.2021890
27. H. Soekmadji, S. Liao, and R. J. Vernon, "Experiment and simulation on TE<sub>10</sub> cut-off reflection phase in gentle rectangular downtapers," *Letters of Progress in Electromagnetics Research*, vol. 12, pp. 79 - 85, 2009. DOI: 10.2528/PIERL09090707
28. H. Soekmadji, S. Liao, and R. J. Vernon, "Trapped mode phenomena in a weakly overmoded waveguiding structure of rectangular cross section," *Journal of Electromagnetic Waves and Applications*, vol. 22, no. 1, pp. 143 - 157, 2008. DOI: 10.1163/156939308783122706